Kinetic modeling of an enzymatic redox cascade *in vivo* reveals cofactor-caused bottlenecks

Sofia Milker,[a] Michael J. Fink,[b] Nikolin Oberleitner,[a] Anna K. Ressmann,[a] Uwe T. Bornscheuer[c], Florian Rudroff*,[a] and Marko D. Mihovilovic[a]

Abstract: This paper describes the development of a kinetic model for the simulation and optimization of an *in vivo* redox cascade in *E. coli,* using a combination of an alcohol dehydrogenase, an enoate reductase, and a Baeyer-Villiger monooxygenase for the synthesis of lactones. The model was used to estimate the concentrations of active enzyme in the sequential biotransformations to identify bottlenecks together with their reasons and how to overcome them. We estimated adapted Michaelis-Menten parameters from *in vitro* experiments with isolated enzymes, and used these values to simulate the change in concentrations of intermediates and products during the *in vivo* cascade reactions. Remarkably, the model indicated the fastest enzyme to be rate-determining due to the unexpectedly low concentration of the active form, opening up reversible reaction channels towards side products. We also provide substantial experimental evidence, that a low intracellular concentration of flavin and nicotinamide cofactors drastically throttled the performance of the *in vivo* cascade.

Introduction

In recent years, enzymatic cascades have gained popularity due to the high compatibility of biocatalysts in a one-pot or whole-cell environment, thereby circumventing the need to purify intermediates, or to install protective groups.[1] Following the guidelines of retrosynthesis in designing artificial pathways, the key transformations can easily be identified, and the connectivity of reactions can be established.[2] This approach, however, does not consider the performance of the pathway quantitatively. So far, optimization required considerable experimental effort to identify problematic steps. Many methods for optimization towards maximum yield and productivity have been successfully applied on enzyme cascades.[3] Their success, however, depended on the straightforward identification of the limiting factor; failing that, the process involved tremendous experimental work. Computational approaches, such as kinetic modeling of *in vitro* or *in vivo* enzymatic reactions, have only been explored in few studies, e.g. cofactor recycling *in vitro,*[4] modeling of the stability of an aldolase,[5] simulation of a three-enzyme cascade system for synthesis of 6-hydroxyhexanoic acid,[6] or a three-enzyme cascade for the biotransformation of sucrose to cellobiose.[7] These studies were important to gain insights into the limiting factors for biotransformation performance, and largely replaced experimental effort, since hypotheses could reliably be tested *in silico*. So far, most enzymatic kinetic models were based either on known concentrations of enzymes with an *in vitro* system,[5, 7] or the enzymes were assumed to be in excess compared to the substrates in the cell.[8] Only few models have taken into account the intracellular concentration of enzymes, mostly simulating natural metabolic pathways.[9]

Here, we developed such a kinetic model based on a well-characterized, but artificial pathway. This reaction cascade was previously used to study the sequential operation of three unrelated redox enzymes with shared cofactors, both *in vitro*,[10] and in a whole-cell system[11] (Scheme 1).

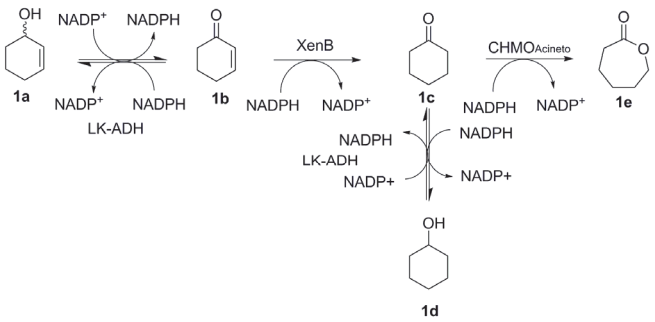

Scheme 1. Cascade reaction from cyclohexenol **1a** to ε-caprolactone **1e**.

It connected the oxidation of a secondary alcohol, a Michael reduction, and a Baeyer-Villiger oxidation, catalyzed by an alcohol dehydrogenase (ADH), an enoate reductase (ERED) and a Baeyer-Villiger monooxygenase (BVMO), respectively.
The ADH (from *Lactobacillus kefir*)[12] depended on magnesium, and the other two enzymes required non-covalently attached flavins as redox-active components (flavin mononucleotide, FMN, for the ERED from *Pseudomonas putida*,[11, 13] and flavin adenine dinucleotide, FAD, for the BVMO from *Acinetobacter calcoaceticus*).[14] The starting material cyclohexenol **1a** was converted to ε-caprolactone **1e** *via* intermediates **1b** (cyclohexanone) and **1c** (cyclohexanone) in the particular

[a] MSc. S. Milker, Dr. N. Oberleitner, Dr. A. K. Ressmann, Prof. Dr. M. D. Mihovilovic, Dr. F. Rudroff
Institute of Applied Chemistry
TU Wien
Getreidemarkt 9/163-OC, 1060 Vienna (Austria)
E-mail: florian.rudroff@tuwien.ac.at
[b] Dr. M.J. Fink
Department of Chemistry and Chemical Biology
Harvard University
12 Oxford St, Cambridge, MA 02138, USA
[c] Prof. Dr. U. T. Bornscheuer
Institute of Biochemistry, Dept. of Biotechnology & Enzyme Catalysis
Greifswald University
Felix-Hausdorff-Str. 4, 17489 Greifswald (Germany)

Supporting information for this article is given via a link at the end of the document.

cascade; the transformation was shown to proceed comparably well on several other examples, including the conversion of (1*S*,5*S*)-carveol **2a** to the corresponding lactone **2e** (Scheme 2). The ADH also catalyzed the redox equilibration between cyclohexanone **1c** and the side product cyclohexanol **1d**.[10] Since all reactions catalyzed by the ADH were reversible at room temperature (25 °C), the formation of intermediate **1d** merely extended the reaction time towards the desired product.

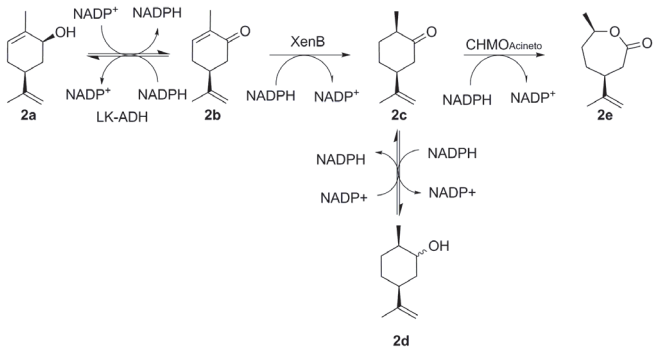

Scheme 2. The cascade example from starting from (1*S*,5*S*)-carveol **2a**.

Within the present study, we aimed at identifying the origin for the reduced productivity, and propose optimization strategies *via* simulations with minimum experimental effort. The specific objectives of the model were (i) to estimate the enzyme concentrations in the reaction to locate the rate-determining step, (ii) to identify possible extrinsic reasons for its reduced velocity within the cascade, and (iii) to propose an optimization strategy to overcome this limitation, and increase the overall performance of the cascade.

Results and Discussion

The rate laws for all cascade reactions were derived based on Michaelis-Menten (MM) theory. We then determined the kinetic parameters *via* initial rate measurements, and used them as constant parameters in non-linear fitting of experimental data from *in vivo* cascades. This way, the concentrations of active enzymes were estimated. The resulting model served to simulate two cascade examples, and to formulate hypotheses pertaining the limiting factors to the performance of the cascade. These hypotheses were then tested both *in silico*, and by experiments *in vitro*.

Development of the kinetic model

First, we postulated the generic rate laws for all reactions, beginning with the starting material **a** (eq. (1)), then the intermediates **b** (eq. (2)) and **c** (eq. (3)), the side product **d** (eq. (4)), and the final product **e** (eq. (5)).

$$(d[a])\,(dt)^{-1} = -\,v_{a\to b} + v_{b\to a} \quad (1)$$

$$(d[b])(dt)^{-1} = v_{a\to b} - v_{b\to a} - v_{b\to c} \quad (2)$$

$$(d[c])(dt)^{-1} = -\,v_{c\to d} + v_{d\to c} + v_{b\to c} - v_{c\to e} \quad (3)$$

$$(d[d])(dt)^{-1} = v_{c\to d} - v_{d\to c} \quad (4)$$

$$(d[e])(dt)^{-1} = v_{c\to e} \quad (5)$$

We assumed that the concentration of the essential cofactors $NADP^+$ and NADPH would remain approximately constant over the course of the reaction *in vivo*, since viable *E. coli* cells would actively regulate the redox balance for homeostasis.[15]
We further assumed that all enzymes would suffice the conditions for Michaelis-Menten kinetics, possibly with inhibition, and calculated the individual rates of the reactions based on Eq S1 (see SI). For all ADH-catalyzed reactions, we added terms for mixed inhibition (Supplementary Eq. S2), since we later observed that the enzyme was inhibited by the initially used co-solvent ethanol (see below). Substitution with the enzyme- and substrate-specific parameters lead to the Michaelis-Menten rate laws, described by Supplementary Eq. S3-S5, for the productive reactions of the cascade and the rate laws for the ADH-catalyzed back and side reactions, described by Supplementary Eq. S6-S8. These equations were later used for non-linear fitting to the experimental data from *in vivo* cascades, after substitution with the parameters from *in vitro* experiments.

Determination of Michaelis-Menten parameters

We measured the initial rates of all reactions in the cascade (Table 1), using a standard protocol (see Experimental Section and the Supplementary Information) with one major adaptation: the nicotinamide cofactors were not supplied in such excess, that all enzymes were saturated, but rather added at the intracellular concentration of *E. coli* (0.12 mM for NADPH, 0.10 mM for $NADP^+$).[16] The resulting estimate for velocity (k_{cat}) was thus not directly comparable to values obtained at saturation. That notwithstanding, the adaptation would increase the meaningfulness of *in vitro* data for the use in modeling of *in vivo* processes.

The highest impact of incomplete saturation by the cofactors was determined for the ADH: the results indicated that it would operate *in vivo* at $0.8\times k_{cat}$ in oxidative direction ($[NADP^+]_{E.\ coli} = 3.3\times K_M$), and at $0.5\times k_{cat}$ in reductive direction ($[NADPH]_{E.\ coli} = 1.2\times K_M$). The difference in K_M values was beneficial to the productive flux of the cascade, including the recovery of the side product **1d** by re-oxidation. The other two enzymes would largely remain unaffected by the low concentration ($[NADPH]_{E.\ coli} = >0.95\times k_{cat}$ for the ERED, $>0.85\times k_{cat}$ for the BVMO).

Table 1. Michaelis-Menten parameters for all enzymatic processes.

ADH				
Substrate	K_M [mM]	$k_{cat,app}$[a] [s^{-1}]	$k_{cat,app}$[a] [s^{-1}]	k_{cat} K_M^{-1} [mM^{-1} s^{-1}]
		oxidation	reduction	
1a	28.5 ± 2.7	11.2 ± 0.8		0.39 ± 0.06
1b	23.6 ± 1.6		4.4 ± 0.2	0.19 ± 0.02
1c[b]	2.7 ± 0.3		78.0 ± 6.9	28.9 ± 5.77
1d[b]	21.3 ± 1.0	14.9 ± 0.6		0.7 ± 0.05
2a	3.6 ± 0.7	0.7 ± 0.1		0.3±0.09
2b	–	No activity detected		
2c	–	No activity detected		
2d	–	Activity towards a mixture of isomers detected		
$NADP^+$	0.03[c]	not applicable	–	–
NADPH	0.14[c]	not applicable	–	–

ERED			
Substrate	K_M [mM]	k_{cat} [s^{-1}]	k_{cat} K_M^{-1} [mM^{-1} s^{-1}]
1b	0.94 ± 0.08	1.53 ± 0.08	1.62 ± 0.22
2b	0.09 ± 0.03	0.22 ± 0.04	2.54 ± 1.30
NADPH	0.0036 ± 0.0005	–	–

BVMO			
Substrate	K_M [mM]	k_{cat} [s^{-1}]	k_{cat} K_M^{-1} [mM^{-1} s^{-1}]
1c	0.0069[d]	22.6[d]	3275.4
2c	0.21 ± 0.03	46.82 ± 3.94	225.0 ± 51.0
NADPH	0.018[d]	–	–

[a] maximum k_{cat} at $NADP^+$ = 0.1 mM, NADPH = 0.12 mM [b] side reaction [c] taken from ref.[12]. [d] taken from ref.[14].

The kinetic parameters were estimated from non-linear fitting of experimental data using the MM-equation. For Michaelis Menten plots see supplementary information (Supplementary Fig. S5-S7). Results estimated with 95% confidence intervals (CI), N=3.

Furthermore, we investigated the influence of ethanol on the performance of the cascade, as it had previously been used to add the substrates to the reaction (0.4 %, approx. 69 mM).[11] Its technical properties as a solvent (stable, benign, water-miscible, bio-compatible, volatile)[17] advocated its use in enzymatic cascades,[18] but as a primary alcohol, it might interfere with the function of ADHs. We observed a mixed type of inhibition, and determined the inhibition parameters K_i = 64.9 mM and K_{ii} = 126.9 mM (Supplementary Eq. S2, Supplementary Fig. S1–S4). These constants were then used for all the rate laws that described ADH-catalyzed reactions.

In the first cascade, all ADH-promoted steps had similar rates and affinity parameters, with the exception of the unproductive reduction of **1c** to **1d**, which proceeded with approx. 100-fold higher catalytic efficiency (k_{cat}/K_M). The high affinity of ADH for **1c** created the possibility of a kinetic dead end, where material was diverted to **1d** quickly, and even at low concentration of **1c**. The side product **1d** would then accumulate because of its low affinity, before being re-oxidized at a slow rate. This unproductive substrate promiscuity could best be mitigated by an efficient final step, catalyzed by the BVMO, thus preventing the build-up of **1c**.

In the second cascade, the ADH only converted the starting material, carveol (**2a**), with no detectable activity for back or side reactions. The other two enzymes had a higher affinity for their respective substrates than the ADH (up to 10^4-fold). The rates of the ERED-catalyzed reactions were the slowest of all steps, whereas the BVMO were the highest in the productive flux.

In summary, the results from *in vitro* kinetics suggested that, at approximately equal concentration of all enzymes, bottlenecks would be caused by the promiscuous activity of the ADH, or by accumulation of intermediates **b** due to the inefficient Michael-addition (ERED).

Modeling of the cascade reactions

We inserted the experimental Michaelis-Menten values as constant parameters into Supplementary Eq. S1–S8, and performed non-linear fitting of this set of differential equations to the previously obtained *in vivo* data by iterative least-squares regression, leaving the concentrations of enzymes as variable parameters to the fit. That implied the assumption that the biocatalysts would not degrade over the course of the reaction. We also omitted any terms for evaporation of the volatile compounds, since the cascade reactions were run in closed vessels.[11] The headspace of the vial was 10×fold higher than the volume of the biotransformation to avoid oxygen limitation. The fitting algorithm estimated the following concentrations: 123 ± 10 µM ADH, 51 ± 5 µM ERED and approx. 0.03 µM BVMO (Figures 1 and 2).

Using these values, we obtained a highly accurate model for both cascades (quantified using adjusted R^2, Table 2), thus validating our mechanistic assumptions and the adapted Michaelis-Menten parameters, with some exceptions.

Table 2. Adjusted coefficients of determination (Adj. R^2) for the comparison of modelled vs experimental data.

Cascade	a	b	c	d	e
1	0.99	0.98	-5.00	0.60	0.98
2	0.91	n.a. [a]	-1.23	n.a. [a]	0.93

[a] n.a = not applicable: the intermediates were not detected in the experiments.

The equation for calculation of adj. R^2 values can be found in the supplementary information (Supplementary Equation S9).

Experimentally, the intermediates **1c** and **2c** only appeared at the first data point, and could not be modelled correctly (negative adj. R^2). Compound **1d** was determined less accurately by the model than the other components, and intermediate **2b** was not detected in the experiment, but was predicted by the model to be present for the first 6 minutes; these errors likely resulted from insufficient precision and sampling frequency in the experimental data.

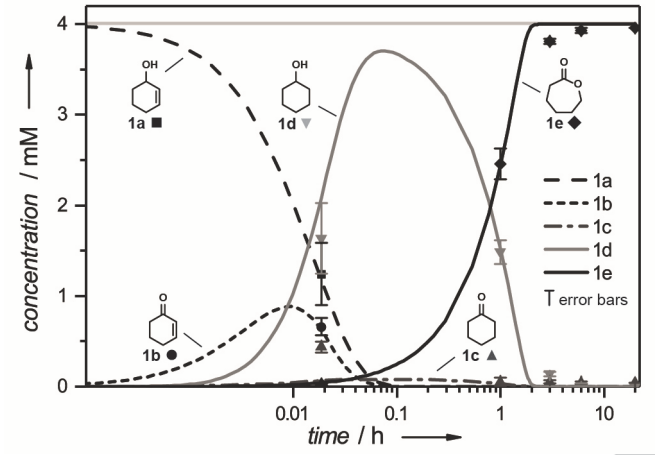

Figure 1. Comparison of experimental (data points) with the simulated (lines) concentrations for cascade **1**. Experimental data were plotted as mean ± 2 SD (standard deviation). Conditions for calculations: 4 mM **1a**,constant concentration of 0.10 mM $NADP^+$ and 0.12 mM NADPH, [ADH] = 123 µM, [ERED] = 51 µM, [BVMO] = 0.033 µM.

Although the misrepresentation of **1c** and **2c** detracted only little from the overall accuracy of the model, it indicated that some of the assumptions were not entirely correct.

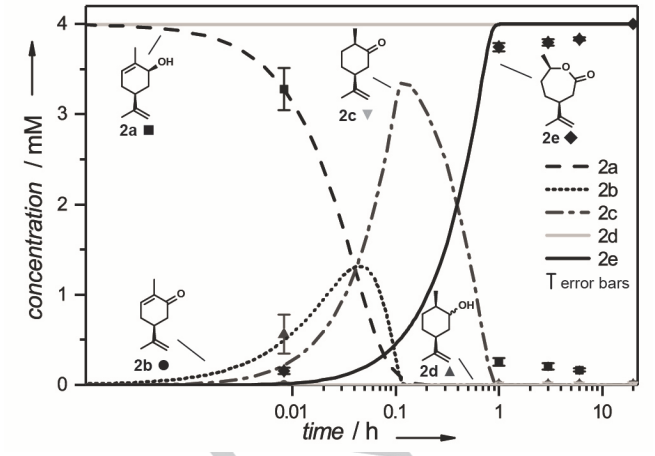

Figure 2. Comparison of experimental (data points) with the simulated (lines) concentrations for cascade **2**. Experimental data were plotted as mean ± 2 SD. Conditions for calculations: 4 mM **2a**,constant concentration of 0.10 mM $NADP^+$ and 0.12 mM NADPH, [ADH] = 123 µM, [ERED] = 51 µM, [BVMO] = 0.033 µM.

Similarly, the model predicted both cascades to complete within 1–2 h, when only approx. 90 % conversion were reached in the experiments within that time; it took another 18 h to reach 100 %. We hypothesized that (i) the equilibration of nicotinamides in *E. coli* was too slow to compensate for the artificial pathway $(d[NADP(H)]/dt \neq 0)$, and (ii) the enzymes' specific activity decreased significantly over the course of the experiment. Whereas the prior case would influence all steps, resulting in a complex effect, the latter scenario would become more apparent at longer reaction times, and later in the cascade (by count of steps). The decelerating rate in the last reaction corroborated that the BVMO was decaying significantly.[19]

Furthermore, we were curious, why the fitting algorithm had estimated the concentration of active BVMO at four to five orders of magnitude lower than of the other two enzymes. Based on the semi-quantitative protein analysis *via* SDS-PAGE, we estimated that the BVMO was present at approx. 10 % of the ERED's mass concentration in the soluble protein fraction of the cell. (Supplementary Fig. S8). That result indicated that the average specific activity of the BVMO over the course of the reaction was much lower than that of the other enzymes, since the model estimated a ratio of approx. 10^4 vs. 10^1 from *in vivo* analysis.

We speculated that most of the total amount of BVMO was inactive in the cell. Thus, we simulated the cascade with increasing titers of BVMO, up to the same order of magnitude as the other two enzymes (>5 µM). The model predicted a complete suppression of the accumulation of **1d** (Fig. 3), and a much shorter reaction time (0.1 h vs. 2.2 h; Supplementary Fig. S9), thereby supporting our hypothesis.

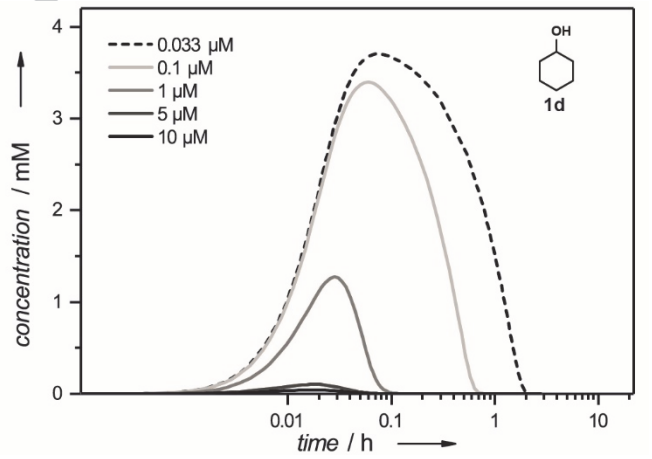

Figure 3. Simulated influence of the BVMO concentration on **1d** formation. 4 mM **1a**, constant concentration of 0.10 mM $NADP^+$ and 0.12 mM NADPH, [ADH] = 123 µM, [ERED]= 51 µM, [BVMO] varied from 0.033–10 µM, Michaelis-Menten parameters can be found in Table 1.

Next, we searched for possible reasons for the low specific activity of the BVMO. We amended our previous hypothesis – that cofactors would not be recycled sufficiently fast – with the assumption that FAD and its precursors would not be in adequate supply to maintain all BVMO in its active, FAD-bound form.

To test this hypothesis, we investigated the effect of excess $NADP^+$/NADPH and flavin nucleotides (FMN/FAD) on the

performance of the cascade *in vitro*. Therefore, we obtained cell-free extracts of the cascade enzymes, simultaneously produced in the same host, and under the same conditions as for the *in vivo* biotransformations. Nicotinamide cofactors were added in stoichiometric excess to the substrates; flavins were added sub-stoichiometric to the ERED, but in excess to the BVMO. We performed two sets of experiments, starting from **1a**: (i) with $NADP^+$/NADPH only (Fig. 4A), and (ii), with $NADP^+$/NADPH and FMN/FAD (Fig. 4B). The concentrations of the enzymes were at the same ratio as the estimates in the model (calculated: 1845 µM ADH, 750 µM ERED, 0.5 µM BVMO). In both experiments, the substrate was added in acetonitrile instead of ethanol to exclude the effects of inhibition.

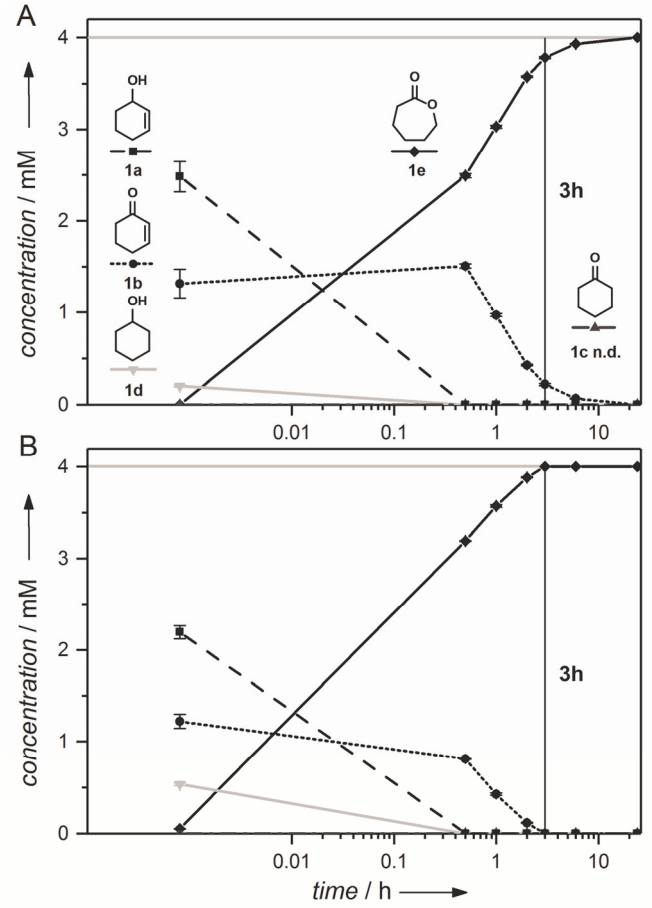

Figure 4. Influence of the cofactors on the *in vitro* cascade biotransformation: A: Stoichiometric amounts of $NADP^+$ and NADPH for the reaction (5 mM each), 4 mM **1a**; B: Stoichiometric amounts of $NADP^+$ and NADPH for the reaction (5 mM each) and addition of FMN and FAD (0.1 mM each) to the cell free extracts, 4 mM **1a**; n.d. not determined.

In the first experiment (Fig. 4A) the byproduct **1d** was detected at a lower concentration, and for a shorter period of time, than in the *in vivo* experiments. That strongly suggested that its accumulation was not only promoted by the suspected low BVMO concentration *in vivo*, but was also caused by an unfavorable balance of the nicotinamides.

In the second experiment (Fig. 4B), which included FMN/FAD, we additionally observed a much shorter reaction time (3 h vs. 24 h *in vivo*); both flavin-dependent enzymes had a higher activity than *in vivo*, with a larger increase for the BVMO than for the ERED.

We speculated that the unequal improvement resulted from the sequence in the biosynthesis of flavin nucleotides: FAD is only produced *via* FMN as a direct precursor. Bound FMN (e.g. to the ERED) would not be available for further conjugation with adenine to form FAD.[20] The amount of available FAD in the cell would thus be lowered by, and proportional to, the ERED, consequently reducing the specific activity of the BVMO. Hence, an excess of FAD should have a stronger influence on the activity of the last enzyme, as seen experimentally. Since our kinetic model did not account for inactive enzyme or stability, the initially fitted value did not reflect the estimated total concentration of BVMO, but only the active fraction.

An immediate solution for a flux improvement would be the addition of cofactors to the cellular system. This is not feasible due to the lack of their cell permeability. Another strategy would be the addition of cofactor precursors like riboflavin which are cell permeable. The group of Stewart[21] investigated the influence of riboflavin addition to a whole-cell BVMO oxidation but no influence on the overall cascade flux was observed. Furthermore the introduction of a more stable BVMO,[22] as recently discovered by Romero *et al*. would be beneficial for the overall flux through the cascade.

In summary we assume, that further flux improvements of our cascade can be achieved by changing the host organism, which provides increased cofactor availability ($NADP^+$/NADPH and FMN/FAD) and applying a more stable CHMO enzyme.

Effect of ethanol on cascade performance

Ultimately, we used the kinetic model to investigate mixed inhibition of ethanol on the ADH (see section on MM parameters). In detail, we tested (i) if ethanol had a significant effect on the performance of the cascade, and if so, (ii) how large that effect was. Our hypothesis was that ethanol would slow down the formation of the final product. Therefore, we simulated the cascade starting from **1a** with a range of ethanol concentrations (0 % to 10 %, Supplementary Fig. S10). At the experimentally used level (0.4 % ethanol), the first reaction was estimated to be slightly slower than without cosolvent (80 mM h^{-1} vs. 53 mM h^{-1}) (Supplementary Fig. S11). Still, the productivity of the whole cascade was not affected at all tested concentrations, since the ADH-catalyzed step was not rate-determining in our system.

Conclusions

We successfully developed an accurate kinetic model for an artificial *in vivo* redox cascade, using adapted Michaelis-Menten parameters from *in vitro* experiments. The concentrations of active enzyme *in vivo* were estimated by non-linear fitting of the rate laws to the experimental data. This way, we could simulate the change in the formation of by-products, and the change in

productivity upon varying the levels of the rate-determining catalyst (large influence), or of the co-solvent (no influence).

More importantly, the model identified a bottleneck resulting from an unexpectedly low specific activity of the last catalyst (BVMO), which was not evident from *in vitro* kinetics and SDS-PAGE analysis of *in vivo* protein titers. We thus argue that the estimation of intracellular enzyme concentrations is an important parameter for the optimization of cascades.

Furthermore we tested our assumption of stable and continuous supply of cofactors (FAD & NADPH) by *E. coli*, suspecting that a lack thereof would have caused the low activity of the BVMO.

An *in vitro* experiment with an excess of cofactors was compatible with this hypothesis, reducing the overall reaction time from 24 to 3 h.

In summary, our findings suggested that the optimization of cascades in a cellular environment should also strongly consider the availability of redox cofactors, their fluxes upon operation of the artificial pathway as well as the amount and stability of all enzymes involved.

WILEY-VCH

Experimental Section

Materials

All chemicals were purchased from Sigma (Steinheim, Germany) or VWR (Hannover, Germany) and were used without further purification unless otherwise specified.

Bacterial strains, plasmids and culture conditions

The enzymatic cascade consists of an alcohol dehydrogenase (ADH) from *Lactobacillus kefir* (LK-ADH[12]), an enoate reductase (ERED) from *Pseudomonas* sp. (XenB[11, 13]) and a Baeyer-Villiger monooxygenase (BVMO), precisely cyclohexanone monooxygenase from *Acinetobacter* sp. ($CHMO_{Acineto}$[14]). All three enzymes were expressed separately in *E. coli* BL21 (DE3). LK-ADH was encoded on a pET22b(+) vector, the XenB on a pGASTON vector and the CHMO on the pET22b(+) vector. For protein production, LB medium (for LK-ADH and CHMO) and TB medium (for XenB) was inoculated from a LB overnight preculture (1:100) with the appropriate antibiotic. The main culture was treated according to the respective expression protocol (media compositions, antibiotics and expression conditions as given in the supplementary information).

Purification of enzymes

After expression the culture was centrifuged (10 min, 5000 × g, 4 °C), the supernatant was discarded and the cells were resuspended in 40× less volume Tris-HCl buffer (50 mM, pH 7.5) containing phenylmethylsulfonyl fluorid (0.1 mM PMSF). Cells were placed on ice and sonicated using a Bandelin KE76 sonotrode connected to a Bandelin Sonoplus HD 3200 in 9 cycles (5 s pulse, 55 s break, amplitude 50 %). Precipitates were removed by centrifugation (15000 × g, 15 min, 4° C).

For the ADH, enrichment was performed by loading the clear supernatant into a centrifugal device with a 50 kDa cut-off and centrifuged to wash all proteins below 50 kDa into the flowthrough. The retained solution was washed twice with Tris-HCl (50 mM, pH 7.5, 50 mM $MgCl_2$) and concentrated to a concentration of around 500 µM.

For poly-His-tag purification (ERED and BVMO), the clear supernatants containing the polyhistidine-tagged enzymes were loaded on a Ni^{2+}-sepharose HP affinity column (1 mL, GE Healthcare bioscience) equilibrated with Tris-HCl buffer (50 mM, pH 7.5, 0.5 M NaCl) Unspecifically bound enzymes were eluted with a binding buffer containing 40 mM imidazole in 7 column volumes. The enzyme of interest was eluted with elution buffer containing 250 mM imidazole in 3 column volumes. Fractions containing the enzymes were identified by SDS-PAGE analysis, pooled and concentrated by ultrafiltration by using ultracentrifugal tubes with a cut-off of 10 kDa (Amicon Ultra, Millipore). For the ADH purification all buffers contained 50 mM $MgCl_2$ and for the BVMO purification, all buffers contained 100 µM FAD.

Determination of the protein concentration

Protein concentrations were determined by the dye-binding method of Bradford at 595 nm using a pre-fabricated assay (BioRad) and bovine serum albumin as the calibration standard.

Determination of kinetic parameters

Activity measurements were performed spectrophotometrically with the Shimadzu UV-1800 photometer at 340 nm by monitoring the initial rates of NADPH formation or depletion in 700 µL cuvettes (ε_{NADPH} = 6.22 mM^{-1} cm^{-1}). The Michaelis-Menten parameters of the ADH were measured in Tris-HCl buffer (50 mM, pH 7.5, 50 mM $MgCl_2$) at 25 °C with different substrate concentrations in triplicates and 0.1 mM for $NADP^+$ (for oxidations) and 0.12 mM for NADPH (for reductions). The enzyme concentration was between 0.8 and 10 µM depending on the velocity of the reaction. The total volume was 500 µL and the measurement was started by addition of cofactor.

For the ERED, the Michaelis-Menten parameters were measured in Tris-HCl buffer (50 mM, pH 7.5) at 25 °C in triplicates. The measurement was started with 0.12 mM NADPH. The enzyme was applied in a concentration of 4 µM and total reaction volume was 500 µL.

For the BVMO, the Michaelis-Menten parameters were determined in Tris-HCl buffer (50 mM, pH 7.5, 0.1 mM FAD) at 25° C in triplicates. The measurement was started with 0.12 mM NADPH. The enzyme was applied in a concentration of 0.05 µM and the total reaction volume was 500 µL.

All substrate stocks were prepared in acetonitrile. For determination of the ethanol effect on the ADH the ethanol was added to the measurements prior to starting the reaction.

The specific activity was calculated according to

$$\text{specific activity } k_{cat} = \text{volumetric activity} \times [ENZ]^{-1}$$

The fitting of the Michaelis-Menten curves to determine kinetic parameters was performed with Origin 2015G.

Mixed inhibition studies

See supplementary information (Supplementary Figures S2-S4).

Biocatalytic screenings

For the *in vivo* reactions of cyclohexenol or carveol as substrate, the *E. coli* BL21 (DE3) with all three enzymes (ADH, ERED and BVMO) in one cell was expressed in TB, supplemented with ampicillin and kanamycin, according to the expression protocol (supplementary information). To the expressed culture 1 % glucose was added and the culture was transferred into vials with 10× higher volume as the volume of the biotransformation. The glass vials were sealed during the reaction, evaporation would be reduced to a minimum. The reaction was started by substrate addition (1 M stock in ethanol) to a final concentration of 4 mM. [11]

For the *in vitro* screening of cyclohexenol (**1a**), the expressed *E. coli* BL21 (DE3) with ADH, ERED and BVMO was centrifuged, resuspended in 15× less Tris-HCl (50 mM, pH 7.5) and divided in two different fractions. One fraction was only supplemented with 0.1 mM PMSF and the other fraction was supplemented with 0.1 mM PMSF and additionally with 0.1 mM FMN and FAD. Both fractions were sonicated on ice using a Bandelin KE76 sonotrode connected to a Bandelin Sonoplus HD 3200 in 9 cycles (5 s pulse, 55 s break, amplitude 50 %). Precipitates were removed by centrifugation (15000 × g, 15 min, 4° C). The supernatant

was applied in a biotransformation with 90 % of the total biotransformation volume (19 mg mL^{-1} enzyme, which is approx. 15 × more concentrated than in the whole-cell reaction mixture). The other 10 % of the biotransformation volume were cofactors, added to the final concentration of 5 mM $NADP^+$ and 5 mM NADPH. The reaction was started by addition of the substrate cyclohexenol (**1a**).

In both cases, the reactions were performed at 20° C with shaking and samples were taken and analysed *via* GC-FID.

GC-analysis

100 µL sample were extracted with 500 µL ethyl acetate supplemented with 1 mM methyl benzoate as internal standard. Conversion was determined by GC using a ThermoQuest Trace GC 2000 with a FID detector equipped with a BGB175 (30 m x 0.25 mm ID, 0.25 µm film).

Model development

The model was developed on the basis of Michaelis-Menten equations for every reaction step of the cascade, including possible back and side reactions for the ADH from initial rate measurements. The model was built in MATLAB 2013b Simbiology Toolbox. The parameter [ENZ] for enzymatic concentration in the different reactions was fitted with nonlinear regression using iterative least squares estimation. [ADH] was fitted to the same value with several different initial values [0.1, 1, 10, 100 µM] in the first round of fitting. In the second round, [ADH] was fixed to the determined value and the other two parameters [ERED]; [BVMO] were fitted with different initial values [0.1 to 100 µM], which always converged on the same results.

Synthesis of (2*R*,5*S*)-dihydrocarvone

To six different batches of non-baffled Erlenmeyer flasks (500 mL) containing 100 mL resting cells expressing XenB, 75 µL of a *S*-(+)-carvone stock (50 mg mL^{-1} in acetonitrile) were added (expression details in the supplementary information). The Erlenmeyer flasks were shaken at 25 °C and 300 rpm. The progress of the reaction was monitored using GC. After 30 min GC showed full conversion and 75 µL of the carvone stock were added. After 1.5 h GC showed full conversion and another 75 µL of the substrate stock were added resulting in a total addition of 700 mg *S*-(+)-carvone.

After 2.5 h total reaction time all batches were extracted three times with diethyl ether and the combined organic layers were dried over Na_2SO_4, filtered off and concentrated *in vacuo*. The crude product was purified using 90 g silica and pentane/diethyl ether (gradient, 0-10 % ether). A colorless oil (88 % yield) was obtained as *cis*:*trans* 8:1 mixture.

GC samples were taken after 30 min of each batch separately: 100 µL of the reaction mixture were added to a 1.5 mL Eppendorf tube containing 200 µL of ethyl acetate (containing 1 mM methyl benzoate as internal standard) and vortexed for 30–35 s and centrifuged for 1 min. The organic layer was desiccated with Na_2SO_4 analyzed by achiral GC. For NMR spectrum see supplementary information (Supplementary Fig. S12).
NMR code: major cis isomer:
^{1}H NMR (400 MHz, $CDCl_3$) δ 1.09 (d, J = 6.9 Hz, 3H, CH3), 1.56 –1.63 (m, 1H), 1.73 (s, 3H, C=CCH_3), 1.79 – 1.90 (m, 3H), 2.35 – 2.46 (m, 2H), 2.51 – 2.66 (m, 2H), 4.69 (m, 1H, C=CH_2), 4.83 (m, 1H, C=CH_2).
^{13}C NMR (100 MHz, $CDCl_3$) δ_C = 15.8, 21.7, 26.5, 30.8, 44.1, 44.3, 44.7, 111.6, 147.0, 214.2.

Analytical data was in accordance with literature values.[23]

Acknowledgements

We thank the FWF (grant no. P-24483-B20 and grant no. I723-N17) and the DFG (grant no. Bo1862/6-1) for financial support. We are also grateful to Prof. W. Hummel (University of Düsseldorf) for supplying the gene encoding LK-ADH.

Keywords: kinetic modeling • biocatalytic cascade • enzyme estimations *in vivo* • cascade optimization • cofactor limitation

[1] a) E. Ricca, B. Brucher, J. H. Schrittwieser, *Adv. Synth. Catal.* **2011**, *353*, 2239-2262; b) J. Muschiol, C. Peters, N. Oberleitner, M. D. Mihovilovic, U. T. Bornscheuer, F. Rudroff, *Chem. Commun.* **2015**, *51*, 5798-5811; c) S. P. France, L. J. Hepworth, N. J. Turner, S. L. Flitsch, *Acs Catal* **2017**, *7*, 710-724.
[2] a) S. G. Warren, P. Wyatt, *Organic synthesis : the disconnection approach*, 2nd ed., John Wiley & Sons Ltd., Chichester, UK, **2008**; b) N. J. Turner, E. O'Reilly, *Nat. Chem. Biol.* **2013**, *9*, 285-288.
[3] a) R. Agudo, M. T. Reetz, *Chem. Commun.* **2013**, *49*, 10914-10916; b) A. M. Kunjapur, Y. Tarasova, K. L. Prather, *J. Am. Chem. Soc.* **2014**, *136*, 11644-11654.
[4] M. C. Hogan, J. M. Woodley, *Chem. Eng. Sci.* **2000**, *55*, 2001-2008.
[5] M. Sudar, Z. Findrik, Đ. Vasić-Rački, P. Clapés, C. Lozano, *J. Biotechnol.* **2013**, *167*, 191-200.
[6] C. Scherkus, S. Schmidt, U. T. Bornscheuer, H. Gröger, S. Kara, A. Liese, *Biotechnol. Bioeng.* **2017**, 10.1002/bit.26258.
[7] C. Zhong, P. Wei, Y.-H. P. Zhang, *Chem. Eng. Sci.* **2017**, *161*, 159-166.
[8] D. Machado, L. R. Rodrigues, I. Rocha, *Bio. Systems.* **2014**, *125C*, 16-21.
[9] a) L. Kuepfer, M. Peter, U. Sauer, J. Stelling, *Nat. Biotech.* **2007**, *25*, 1001-1006; b) J. Hassan, L. L. Bergaust, L. Molstad, S. de Vries, L. R. Bakken, *Environ. Microbiol.* **2016**, *18*, 2964-2978.
[10] N. Oberleitner, C. Peters, F. Rudroff, U. T. Bornscheuer, M. D. Mihovilovic, *J. Biotechnol.* **2014**, *192*, 393-399.
[11] N. Oberleitner, C. Peters, J. Muschiol, M. Kadow, S. Saß, T. Bayer, P. Schaaf, N. Iqbal, F. Rudroff, M. D. Mihovilovic, U. T. Bornscheuer, *ChemCatChem* **2013**, *5*, 3524-3528.
[12] A. Weckbecker, W. Hummel, *Biocatal. Biotransformation* **2006**, *24*, 380-389.
[13] C. Peters, R. Kölzsch, M. Kadow, L. Skalden, F. Rudroff, M. D. Mihovilovic, U. T. Bornscheuer, *ChemCatChem* **2014**, *6*, 1021-1027.
[14] N. A. Donoghue, D. B. Norris, P. W. Trudgill, *Eur. J. Biochem.* **1976**, *63*, 175-192.
[15] S. Spaans, R. Weusthuis, J. Van Der Oost, S. Kengen, *Front. Microbiol.* **2015**, *6*, 742.
[16] a) K. B. Andersen, K. von Meyenburg, *J. Biol. Chem.* **1977**, *252*, 4151-4156; b) B. D. Bennett, E. H. Kimball, M. Gao, R. Osterhout, S. J. Van Dien, J. D. Rabinowitz, *Nat. Chem. Biol.* **2009**, *5*, 593-599.
[17] F. J. Weber, J. A. M. de Bont, *Biochim. Biophys. Acta. Rev. Biomembr.* **1996**, *1286*, 225-245.
[18] Y. L. Khmelnitsky, V. V. Mozhaev, A. B. Belova, M. V. Sergeeva, K. Martinek, *Eur. J. Biochem.* **1991**, *198*, 31-41.
[19] H. L. van Beek, H. J. Wijma, L. Fromont, D. B. Janssen, M. W. Fraaije, *FEBS Open Bio* **2014**, *4*, 168-174.
[20] C. A. Abbas, A. A. Sibirny, *Microbiol. Mol. Biol. Rev.* **2011**, *75*, 321-360.
[21] A. Z. Walton, J. D. Stewart, *Biotechnol. Progr.* **2004**, *20*, 403-411.
[22] E. Romero, J. R. G. Castellanos, A. Mattevi, M. W. Fraaije, *Angew. Chem. Int. Ed.* **2016**, *55*, 15852-15855.

[23] D. H. Hua, S. Venkataraman, *J. Org. Chem.* **1988**, *53*, 1095-1097.

WILEY-VCH

Entry for the Table of Contents (Please choose one layout)

FULL PAPER

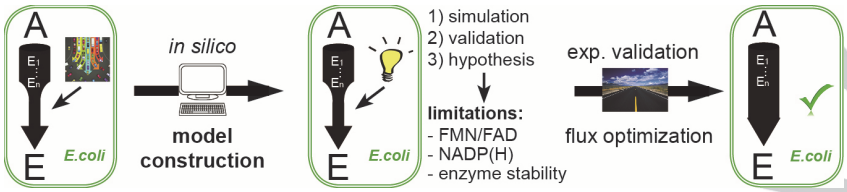

Sofia Milker, Michael J. Fink, Nikolin Oberleitner, Anna K. Ressmann, Uwe T. Bornscheuer, Florian Rudroff and Marko D. Mihovilovic*

Page No. – Page No.

Kinetic modeling of an enzymatic redox cascade *in vivo* reveals cofactor-caused bottlenecks

WILEY-VCH